Development of a Biologically Relevant Calcium Phosphate Substrate for Sum Frequency Generation Vibrational Spectroscopy

Sarah J. McGall[†] and Paul B. Davies*

Department of Chemistry, University of Cambridge, Lensfield Road, Cambridge, CB2 1EW, United Kingdom

David J. Neivandt

Department of Chemical and Biological Engineering, The University of Maine, Orono, Maine 04469

Received: May 16, 2005; In Final Form: August 6, 2005

A novel biologically relevant composite substrate has been prepared consisting of a calcium phosphate (CaP) layer formed by magnetron sputter-coating from a hydroxyapatite (HA) target onto a gold-coated silicon substrate. The CaP layer is intended to mimic tooth and bone surfaces and allows polymers used in oral care to be deposited in a procedure analogous to that used for dental surfaces. The polymer cetyl dimethicone copolyol (CDC) was deposited onto the CaP surface of the substrate by Langmuir Blodgett deposition, and the structure of the adsorbed layer was investigated by the surface specific technique of sum frequency generation (SFG) vibrational spectroscopy. The gold sublayer provides enhancement of the SFG signal arising from the polymer but plays no part in the adsorption of the polymer. The surface morphology of the substrate was investigated using SEM and AFM. The surface roughness was commensurate with that of the thermally evaporated gold sublayer and uniform over areas of at least 36 μm^2. The chemical composition of the CaP-coated surface was determined by FTIR and TOF-SIMS. It was concluded that the surface is primarily calcium phosphate present as a mixture of amorphous, non-hydroxylated phases rather than solely stoichiometric hydroxyapatite. The SFG spectra from CDC on CaP were closely similar, both in resonance wavenumbers and in their relative intensities, with spectra of thin films of CDC recorded directly on gold. Application of previous analysis of the spectra of CDC on gold therefore enabled interpretation of the polymer orientation and conformation on the CaP substrate.

Introduction

In recent years, the spectroscopic technique of sum frequency generation (SFG) vibrational spectroscopy has been increasingly applied to investigate the interfacial properties of biological systems, with a particular emphasis on protein adsorption. For example, Wang et al. have studied bovine serum albumin (BSA) adsorption in a number of systems, including at aqueous/air, aqueous/silica, and aqueous/polystyrene interfaces.[1−3] The relative intensities and phases of the C−H SFG resonances of BSA displayed a marked dependence upon the interface employed, indicating significant surface specific changes in the adsorbed conformation of the protein. In a subsequent publication, the same group performed a complementary study of the effect of protein adsorption on the conformational order of a polymeric substrate.[4] Kim et al. have probed the effect of pH on the conformation of hen egg white lysozyme and its associated water at both the quartz/water and air/water interfaces.[5] Somorjai and co-workers have studied the interaction of fibrinogen with various synthetic polymeric surfaces[6] and the molecular packing of lysozyme, fibrinogen, and BSA on silica and polystyrene.[7] In a significant development, Watry et al. recently demonstrated the applicability of SFG for determining interfacial orientation and conformational information of nucleic acid-based polymers at an oil/water interface.[8]

All of the above studies were performed on nonbiological substrates due to practical constraints limiting the types of interfaces that may be probed by SFG. For example, if coherent spectroscopy rather than scattering is to be performed, then substrates must meet surface roughness limitations. Further, care must be taken to avoid sample damage induced by the high-energy input laser pulses required for SFG. Finally, the substrate should incorporate a metallic coating of preferably gold or silver that leads to enhancement of the emitted SF signal, while providing a phase reference allowing determination of absolute molecular orientation of adsorbed interfacial species. Over a period of several years, the authors have developed and characterized a methodology for preparing such substrates for nonbiological materials.[9−13] The general approach has been to construct a composite substrate comprising a metal film upon which a thin layer of the substrate material of interest is created. The thickness of the substrate layer is determined by the deposition methodology and the optical properties of the material. The visible and infrared beams required for SF generation are incident upon the substrate/sampling medium interface, and the resulting emitted SFG beam is recorded in a reflection geometry. To date, composite substrates comprising gold/mica,[9,10] gold/polymer,[13] and gold/ Langmuir Blodgett multilayer arachidic acid films[11,12] have been employed. An optical interference effect with a dependence upon the thickness of the substrate material layer has been characterized both theoretically and experimentally.[9−13] In the present study, this methodology is extended to a composite substrate suitable for

* To whom correspondence should be addressed. Tel.: +44 1223 336460. Fax: +44 1223 336362. E-mail: pbd2@cam.ac.uk.

[†] Present address: Procter & Gamble Technical Centres Ltd., Whitley Road, Longbenton, Newcastle upon Tyne NE12 9TS, UK.

10.1021/jp0525742 CCC: $30.25
Published on Web 09/10/2005

SFG that is of high biological relevance, calcium phosphate/hydroxyapatite on gold.

Hydroxyapatite (HA) is a calcium phosphate-based ceramic with the molecular formula $Ca_{10}(PO_4)_6(OH)_2$. HA is chemically and crystallographically similar to the mineral phase of teeth and bone.[14] The simplest means of generating a composite substrate from such a material is to employ a chromium or titanium primed polished silicon wafer as a support, to coat the wafer with a layer of gold several hundred nanometer thick, and finally to deposit a layer of HA, the thickness of which should be less than 100 nm to limit complications arising from the interference effect described above. Depositing chromium and gold on silicon wafers may be achieved by any number of common methodologies; depositing HA, however, is more challenging. A significant number of studies exist on the development of HA coating methodologies, primarily for biomedical applications due to the biocompatibility of HA and its ability to chemically bond to bone.[15] The most widely employed technique for HA deposition is plasma spraying[15−17] in which fused HA powders are ejected through a plasma jet onto a substrate, thereby producing an instantaneous coating. The high temperatures involved, however, result in a film with a composition which deviates from stoichiometric HA, typically by depletion of OH^- ions from the lattice.[16] Further, the adherence of the coating to the substrate, the uniformity of the coating thickness, and the integrity of the structure are often poor.[15] The plasma spraying technique has an additional drawback in the creation of a composite SF substrate; the coatings produced are at least a micrometer thick,[18] far larger than the 100 nm or less required for SFG.

An alternative HA deposition methodology is radio frequency (RF) magnetron sputtering.[19] This method utilizes a gaseous plasma (generally argon) to remove material into the gas phase from a negatively charged target. The material is then deposited on a substrate placed in close proximity to the target.[17] Uniform coatings may be produced with thicknesses ranging from nanometers to micrometers, depending on the sputtering rate employed.[15] However, the chemical composition of the film is extremely sensitive to the sputtering parameters (for example, gas pressure and RF power), and several studies have been performed in an attempt to optimize these parameters. For example, van Dijk et al. have investigated the influence of argon pressure,[20] discharge power level,[15] and the addition of oxygen[21] on the film composition. The stoichiometry of the coatings was found to differ from bulk HA; specifically the Ca/P ratio remained too high even after rigorous optimization of the protocol.[18] This was attributed to the target itself being a plasma sprayed layer of HA on a copper base plate, which as mentioned above is expected to have a stoichiometry that deviates from bulk HA. While dense crystalline HA targets were preferred, they were found to crack during deposition.[18] X-ray diffraction spectroscopy of the sputtered layers indicated that they were amorphous,[17] while annealing was found to induce crystallinity.[17] Annealing at temperatures above 600 °C caused cracks to appear in the coatings, while annealing at 400 °C was found not to alter the amorphous HA structure. Reflection absorption infrared spectroscopy (RAIRS) analysis revealed a large water signal in the amorphous spectrum. After annealing at 500 °C, the water content disappeared and O−H bands became visible in the vibrational spectrum. Consequently, annealing at 500 °C was included in the final protocol.[18] Biological evaluations of the sputtered HA layers revealed their biocompatibility to be excellent with the coating enhancing the growth of hydroxyapatite in a cell culture. No degradation of the layer was observed after a significant length of time.[22−25] Recently, Love et al. have attempted to optimize the sputter coating parameters for HA through development of a system to probe residual gases present during deposition.[26] Powdered HA targets were used. No significant variations in the residual gases present, as a function of discharge power level and argon pressure, were observed with only subtle changes detected in the coatings.

For the present work, the optimized protocols of van Dijk et al. and Love et al. were followed as closely as possible to create HA/gold composite substrates. The HA film was characterized in terms of its thickness, surface morphology, and chemical composition. The characterized substrate was then employed as a model for tooth enamel to measure SFG spectra of a deposited comb copolymer, cetyl dimethicone copolyol (CDC), a polymer employed in the oral care industry for the inhibition of protein adsorption and bacterial adhesion.[27,28] The SFG spectra are interpreted in terms of the orientation of the polymer backbone and its substituent side chains by comparison with previously recorded spectra of CDC on a gold substrate.[13]

Experimental Section

Polished silicon wafer supports (approximately 10 × 15 mm) were cleaned via the following protocol: immersion in a Decon 90 surfactant solution for 24 h, copious rinsing with 18.2 MΩ cm ultrapure water, immersion in concentrated nitric acid for 24 h, and further copious rinsing. The silicon wafer pieces were then mounted in a custom-built sample holder employing stainless steel tweezers (cleaned following the same procedure as above) and inserted into the chamber of a BOC Edwards Auto 500 sputter-evaporator. The chamber was then evacuated to a pressure of 2×10^{-7} mbar and a ∼5 nm thick layer of chromium followed by a ∼150 nm thick layer of gold thermally evaporated onto the surface. Deposition layer thicknesses were determined via a calibrated quartz crystal thickness monitor. Without breaking vacuum, the calcium phosphate layer was then RF magnetron sputtered onto the gold-coated silicon substrate. The sputtering parameters were chosen on the basis of the optimization studies of van Dijk et al. and Love et al. described earlier. A RF power of 300 W was employed. Sputtering was performed for a total of 30 min, with an approximate target to substrate distance of 10 cm. The substrate holder was rotated during deposition. Argon was used as the plasma working gas, and the chamber pressure was held at approximately 1.5×10^{-2} mbar. The sputtering target was custom-made at Testbourne Ltd., Hampshire, UK, by sintering powdered hydroxyapatite. The calcium content of the target was determined to be 36% as compared to a theoretical value of 40% for stoichiometric hydroxyapatite. As discussed above, previous studies of RF magnetron sputtered hydroxyapatite have indicated that it is difficult to reproduce the exact stoichiometry of hydroxyapatite following deposition,[18,26] and therefore the quoted deficiency in calcium content of the target was deemed acceptable.

Ellipsometric measurements of the thickness of the sputtered HA layers were performed on an ELX-02C DRE single wavelength ellipsometer at a wavelength of 632.8 nm and an angle of incidence of 70°. Data were analyzed employing a two-layer model of gold/HA incorporating multiple reflections. The gold refractive index was obtained by performing an ellipsometric measurement on an uncoated gold substrate. The literature refractive index for crystalline hydroxyapatite of 1.64 was employed to determine the HA film thickness.[29] Varying the HA refractive index value between 1.6 and 1.7 resulted in calculated film thicknesses with ∼10% uncertainty.

Scanning electron microscopy (SEM) was performed employing a JEOL 6340F SEM equipped with a field emission

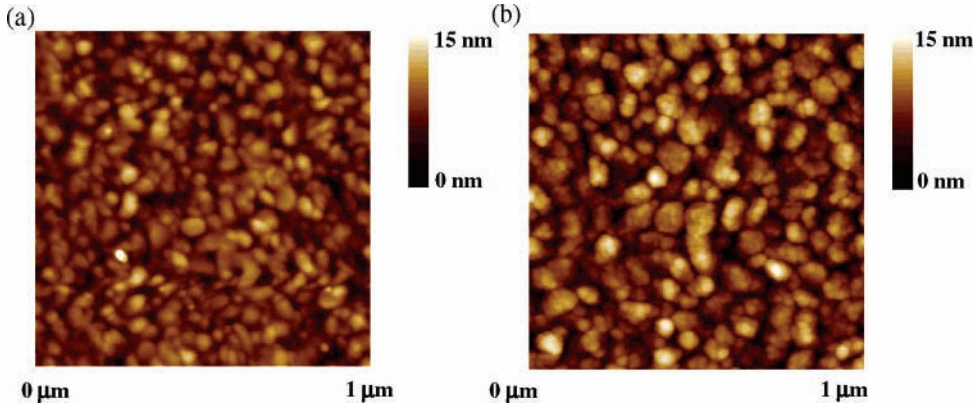

Figure 1. AFM images (1 μm × 1 μm) of the composite substrate. (a) Thermally evaporated gold layer on a chromium primed silicon wafer. (b) Following RF magnetron sputtering of a calcium phosphate film onto a gold-coated silicon wafer. The height ranges are indicated on the color-coded bars.

gun. Images were recorded at magnifications of ×20 000 and ×40 000. Surface charging effects were avoided by limiting the accelerating voltage to 5 kV. Complementary topographical information was obtained using atomic force microscopy (AFM). Specifically, a Digital Instruments Nanoscope IV AFM, with NSC15 silicon cantilevers manufactured by Mikromasch, was employed. Images were recorded in tapping mode with a typical frequency just below the resonance frequency of the cantilever of ~325 kHz. Images were recorded in both height and phase modes across surface areas of 500 nm × 500 nm up to 2 μm × 2 μm. The images recorded across areas of 1 μm × 1 μm were considered to be the most visually informative and are therefore presented here.

Infrared spectra of the HA target (a portion ground into powdered form) and of the deposited HA films were recorded in the ATR mode employing a Specac Golden Gate single reflection ATR accessory (MK11) in conjunction with a Thermo-Nicolet FTIR spectrometer. A 45° angle of incidence diamond internal reflection element (IRE) with a sampling area of 1 mm^2 was used. Samples were mounted in the ATR accessory and clamped with a sapphire anvil against the diamond IRE with a load of 80 lbs. Given that the refractive index of diamond is 2.4[30] and assuming a HA refractive index of 1.64,[29] the predicted penetration depth of the evanescent wave is of the order of 2 μm at 2000 cm^{-1}. Because the deposited HA layer thickness is expected to be less than 100 nm, the evanescent wave is assumed to sample the full film thickness. Difficulties were encountered in reproducibly obtaining good quality spectra of the HA layer of composite substrates, presumably due to insufficient contact with the IRE. Consequently grazing angle FTIR was employed for these samples using a Specac grazing incidence accessory in conjunction with a Bio-Rad FTS 6000 FTIR spectrometer. Incident p polarized light was selected, and spectra were recorded with an incident angle of 85°. Typically 1024 scans were co-added to obtain spectra between 500 and 4000 cm^{-1} with satisfactory signal-to-noise ratios.

Complementary information on the chemical composition of the sputtered layer was obtained via time-of-flight secondary ion mass spectroscopy (TOF-SIMS). Spectra were recorded on an ION-TOF IV instrument made available by Procter & Gamble, Cincinnati, OH. The primary ion used was Ga^+, with a primary ion dose of 6.2×10^7 over 10 s across a sample area of 100 μm × 100 μm, which is expected to be well within the static regime. Because the sample was an insulator, it was flooded with low energy electrons between pulses of primary ions to minimize charge build-up, which would affect secondary ion sputtering efficiencies.[31] It was necessary to produce samples in the UK and ship them to the U.S. It is likely that a small amount of unavoidable surface contamination occurred in transit. No cleaning of samples prior to the recording of TOF-SIMS spectra was undertaken. No comparison of sputtering yields for a specific species across different samples has been performed in this work due to the many factors that may affect the transition probability. The nanosecond sum frequency generation spectrometer used to record spectra in the C−H stretching region between 2800 and 3000 cm^{-1} has been described in detail elsewhere.[32,33]

Langmuir Blodgett (LB) films of CDC were deposited onto composite substrates employing a PTFE LB trough (Nima 611). A 1 mg/mL solution of CDC in chloroform was prepared, and 50 μL was spread at the air/water interface (18.2 MΩcm Milli-Q water, pH ≈ 7). The chloroform was allowed to evaporate for 10 min prior to film compression. Surface pressures were measured using Wilhelmy plates composed of Whatman Chr1 paper. LB layers were deposited by compressing the CDC film to the desired surface pressure (28 mN/m) followed by withdrawing the substrate vertically through the interface into air. The surface pressure was maintained at the desired value throughout the deposition process.

Cetyl dimethicone copolyol, CDC (MW ≈ 12 400) was supplied by Procter and Gamble Technical Centres Limited, UK. The molecular structure of CDC is given in Figure 1 of ref 13. CDC was custom synthesized by randomly grafting a known average number of side chains of C14 alkyl and PEO onto a poly(dimethylsiloxane), PDMS, backbone. The polymer was used as received.

Results and Discussion

Sputtered Layer Thickness and Surface Morphology. Ellipsometric thicknesses of sputtered CaP films were taken at three places across individual samples, one close to the clamped end, one in the center, and one at the unclamped end. A trend of increasing film thickness was observed with distance from the clamped end, for example from 40 ± 4 to 47 ± 5 nm for a representative composite substrate. This observation is presumably due to a shielding effect from the substrate holder. The CaP film thickness of less than 100 nm is within the range desired for minimization of film thickness related interference effects in SFG spectra.

Figure 1a presents a 1 μm × 1 μm AFM height image of a thermally evaporated gold layer on a chromium primed silicon wafer. It may be seen that the surface consists of randomly

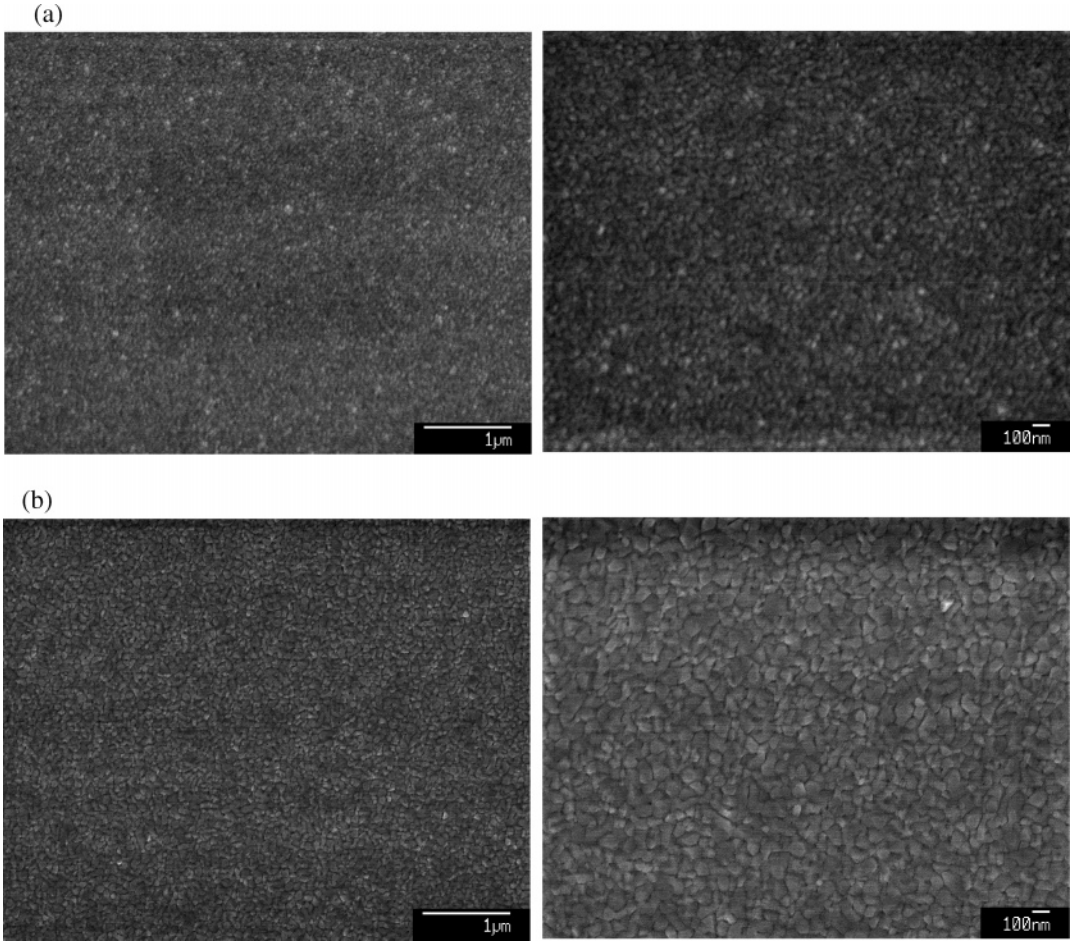

Figure 2. SEM images of the composite substrate. (a) Thermally evaporated gold layer on a chromium primed silicon wafer. (b) Following RF magnetron sputtering of a calcium phosphate film on the gold-coated silicon wafer. The images are displayed at magnifications of 20 000 and 40 000, as illustrated by the scale bars.

arranged clusters of gold. Analysis of the surface morphology (*z*-axis range) reveals that the maximum peak to trough surface roughness is 15.1 (estimated uncertainty ±0.1 nm) within the 1 μm^2 imaging area. Such substrates are routinely employed for SFG and are sufficiently smooth to enable coherent spectroscopy.[12,33−40] Figure 1b is a representative AFM image (1 $\mu m \times 1$ μm) of a composite substrate, comprising a gold-coated chromium primed silicon wafer (such as that of Figure 1a) upon which a layer of CaP has been sputter coated. Comparison of Figure 1a and b reveals that the surface morphology is considerably different. The sputtered CaP layer appears to consist of larger particles than the gold surface, although again the distribution and packing appear to be random. Analysis of the height profile reveals that the maximum peak to trough surface roughness is 16.1 ± 0.1 nm within the 1 μm^2 imaging area, approximately 1 nm (6%) greater than the underlying gold surface. It is concluded that the minor increase in surface roughness of the CaP over the gold surface is likely to be low enough to facilitate ready SFG spectroscopy. On the other hand, it is clear that the gross surface morphology is dictated by the underlying surface of gold particles, and replacement with an atomically flat surface such as template stripped gold[41,42] should in turn provide a much flatter coating of CaP.

The uniformity of the composite substrate in relation to the underlying gold surface was examined on a larger scale via SEM. Figure 2a presents SEM images of the gold surface at magnifications of ×20 000 and ×40 000, as illustrated by the scale bar. Figure 2b presents comparable images of a representative composite gold/CaP substrate. Comparison of the images reveals that the CaP primary particle is considerably larger than the gold primary particle size, a finding consistent both qualitatively and quantitatively with the AFM analysis. Further, it is noted that the gold and sputtered CaP layers appear to be uniform across the imaging area of approximately 36 μm^2. Images recorded at different positions on the same substrate, corresponding to slightly different CaP layer thicknesses, showed similar surface morphologies. Consequently, the combination of ellipsometric, AFM, and SEM analyses of the composite substrate lead to the conclusion that the CaP film thickness, surface roughness, and macroscopic uniformity are acceptable for the application of SFG.

Chemical Composition of the Sputtered Layer. FTIR has been used extensively to probe the chemical nature of deposited calcium phosphate films[14,26,43−49] and synthetic calcium phosphate powders.[46,50−52] A cursory inspection of an IR spectrum of calcium phosphate reveals the presence of phosphate bands at approximately 600 and 1000 cm^{-1}, while bands occurring at approximately 630 and 3570 cm^{-1} indicate the presence of hydroxyl groups in the deposited layer (see references above). Further insight into the detailed composition of the material may be obtained from a closer examination of the FTIR spectrum. For example, the appearance of several sharp, well-defined resonances in the region 950−1100 cm^{-1} is indicative of highly crystalline calcium phosphate, while a single broad resonance in this region indicates a predominantly amorphous phase.[17,43,46,53] This observation is attributed to the coupling of PO_4^{3-} vibrational motions within the crystalline lattice resulting in the

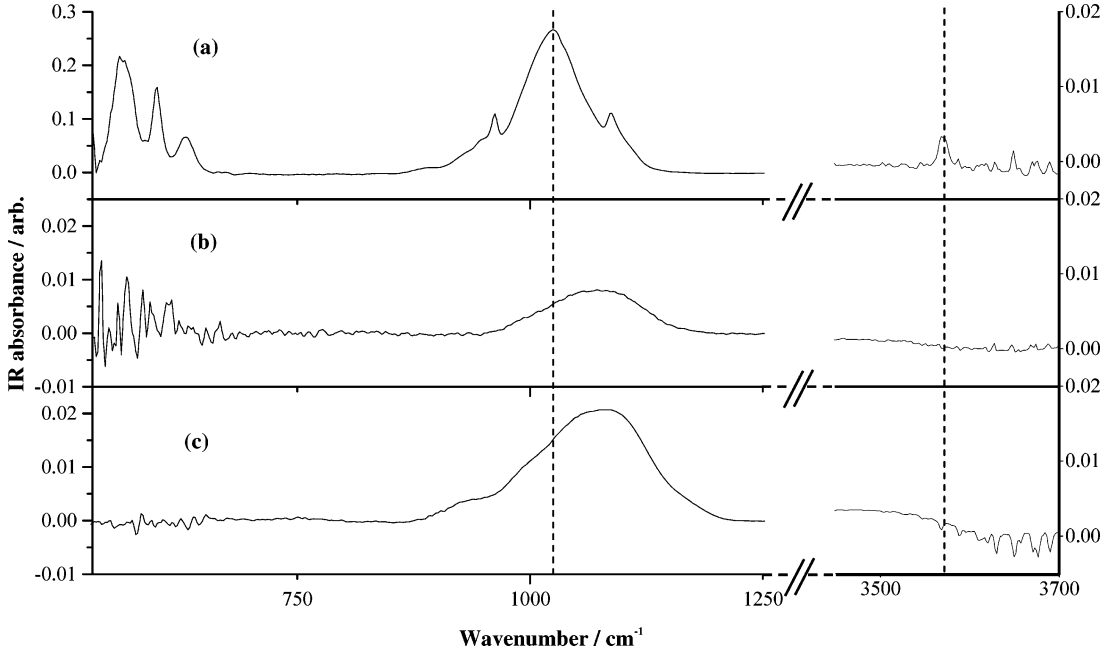

Figure 3. FTIR spectra of the calcium phosphate target and the sputtered layer. Band assignments are given in the text and in Table 1. (a) ATR spectrum of the target, full scale. (b) ATR spectrum of the sputtered film. (c) Grazing angle spectrum of the sputtered film.

TABLE 1: Vibrational Band Positions and Assignments for Powdered Hydroxyapatite (HA) and Deposited Calcium Phosphate (CaP) Layers, As Compared to Spectra Recorded in the Present Work (Last Two Columns)[a]

band assignment	powdered HA[46]	powdered HA[51]	powdered HA[52]	RF sputtered CaP[53]	plasma coated CaP[46]	CaP target Figure 3a	CaP layer Figure 3b,c
ν_2 (P−O)	470	462	437		434		
		474	474		471		
ν_4 (P−O)	565	565	571	567	550	563	
	571	574		587	571		
	601	602	603		604	600	
ν_1 overtone (O−H)	631	631	633	621		630	
ν_1 (P−O)	962	962	961	948, 965		963	950
ν_3 (P−O)	1030	1035		1009	994	1025	
	1062	1065	1047	1083	1074	1087	1077
	1090	1088	1092	1124	1117		
ν_s lattice stretch (O−H)	3573		3568	3571	3571	3570	

[a] ν_1, nondegenerate P−O stretch; ν_2, doubly degenerate O−P−O bending mode; ν_3, triply degenerate antisymmetric P−O stretch; ν_4, triply degenerate O−P−O bending mode.

splitting of predicted degenerate phosphate bands.[46] Further, the hydroxyl bands mentioned above are generally only observed from spectra of crystalline HA layers;[17,26,43,45−47,49−51,53] for example, the band at 3570 cm^{-1} has been assigned to stretching vibrations of hydroxyl groups within the crystalline lattice.[46] Due to the strong dependence of observable vibrational bands, their positions, and relative intensities upon the stoichiometry and crystallinity of hydroxyapatite, the presence of calcium phosphate in its amorphous and crystalline hydroxyapatite phases may consequently be determined by comparison of a recorded spectrum to those in the literature.[46,52] However, to our knowledge, no comprehensive study has been reported that would allow identification and quantification of other calcium phosphate phases that may be present in a sample such as amorphous calcium phosphate ($Ca_3(PO_4)_2 \cdot 3H_2O$), anhydrous dicalcium phosphate ($CaHPO_4$), dicalcium phosphate dihydrate ($CaHPO_4 \cdot 2H_2O$), tricalcium phosphate ($Ca_3(PO_4)_2$), or octacalcium phosphate($Ca_8H_2(PO_4)_6 \cdot 5H_2O$).[14,54]

Figure 3a presents an infrared ATR spectrum of the sputtering target (ground into powdered form). The wavenumbers of the bands observed in the spectrum are summarized in Table 1, as are literature wavenumbers and assignments for bands of powdered crystalline hydroxyapatite (HA) and calcium phosphate (CaP) films deposited via RF sputtering and plasma coating. Inspection of Table 1 reveals that the majority of the resonances typically observed in crystalline HA are present in the IR spectra of the sputtering target. In particular, the position of the ν_1(P−O) nondegenerate stretch observed at 963 cm^{-1} correlates well with the literature value of 961−962 cm^{-1}. The ν_2 O−P−O bending modes predicted to occur in the 437−474 cm^{-1} region are below the optical cutoff of the diamond ATR accessory and hence are not observed. The highest and lowest wavenumber ν_3 bands in the spectrum of the sputtering target occur at positions comparable to those reported in the literature (1025 vs 1030−1035 cm^{-1} and 1087 vs 1088−1092 cm^{-1}). However, the strongest ν_3 component in a majority of the reported spectra of crystalline hydroxyapatite (see references given in Table 1), appearing between 1050 and 1060 cm^{-1}, is not observed here. It is noted that in deposited layers where there are likely to be additional calcium phosphate phases present, it is the positions and intensities of these ν_3 bands that are most strongly affected; see the representative data of Table 1. The two ν_4 bending modes observed at 563 and 600 cm^{-1} are in excellent agreement with the literature values (565−571 and 601−603 cm^{-1}). The third ν_4 mode, expected to occur in the region 571−574 cm^{-1}, may be unresolved due to convolu-

tion with another nearby strong ν_4 mode at 563 cm^{-1}. The positions of the two O−H bands are also in excellent agreement with the literature (630 vs 631−633 cm^{-1} and 3570 vs 3568−3573 cm^{-1}). Consequently, it is concluded that the sputtering target is comprised primarily of crystalline HA. However, it is likely that other calcium phosphate phases and stoichiometries are present, a fact consistent with the known stoichiometric deficiency of the target of ∼4% in Ca.

Figure 3b and c presents ATR and grazing angle infrared spectra, respectively, of sputtered CaP films. In common with the spectra of the target, the most significant feature of the sputtered film spectra are the P−O ν_3 modes centered at 1077 cm^{-1}. In contrast to the target spectra, however, the ν_3 modes of the sputtered film are not resolved but rather appear as a single broad band. Further, the band position of the deposited films is blue shifted by approximately 50 cm^{-1}. This is most likely due to a change in the relative intensities of the ν_3 bands present. It is well recognized in the literature that all of the major coating processes employed for calcium phosphate film deposition (plasma spraying, pulsed laser deposition, RF magnetron sputtering) alter the amount of the amorphous phase present, in addition to the stoichiometry.[18,45,55] These effects, in addition to the stress placed on the crystal structure as a result of dehydroxylation and/or displacement of hydroxyl ions in the structure due to nonequilibrium coating processes,[46] result in significant variation in the IR spectra of calcium phosphate films deposited by different methods and indeed by the same method but under different conditions. The lack of a comprehensive study on the nature of deposited calcium phosphate layers means that it is difficult to draw conclusions with regards to the exact phases present in the deposited layers. It may, however, be concluded that a primarily amorphous layer has been deposited, as expected from literature reports of RF magnetron sputtering of hydroxyapatite.[17] Further evidence for the amorphous nature of the sputtered film is the lack of O−H resonances in the spectra (∼630 and 3570 cm^{-1}).

Following the protocol of van Dijk et al., an attempt was made to induce crystallinity by annealing the calcium phosphate films at up to 600 °C for a period of approximately 3.5 h.[17] Visual inspection of the annealed films revealed that they were dull and patchy. The most likely explanation is that the underlying gold layer and the calcium phosphate layer have diffused into each other at elevated temperatures to create a mixed film. This film did not yield the expected strong nonresonant background SFG signal. It was concluded therefore that routinely annealing the films to obtain more crystalline calcium phosphate is not practical or appropriate for the composite gold/CaP substrates.

TOF-SIMS has been employed to complement the compositional characterization of the deposited film by FTIR, described above. Several recent studies have reported the successful application of TOF-SIMS for investigation of the chemical nature of HA powders[54,56−58] and layers.[54,56,59−63] Mass peaks characteristic of calcium phosphate phases have been identified including Ca^+, CaO^+, $CaOH^+$, O^-, OH^-, PO^-, PO_2^-, and PO_3^-. The first comprehensive TOF-SIMS study of different calcium phosphate phases in powder form was reported by Chuseui et al.[57] The ratio of PO_3^- and PO_2^- secondary ions was found to differ for most of the calcium phosphate phases except hydroxyapatite and tricalcium phosphate, in which they were closely similar (statistically identical). Subsequently the PO_3^-/PO_2^- secondary ion ratio was used to identify the CaP phases deposited onto a titanium oxide substrate from a calcium phosphate aqueous solution. More recently, Lu et al. built on this work by using principal component analysis to differentiate between different calcium phosphate phases.[58] Yields of PO_3^-, PO_2^-, O^-, OH^-, Ca^+, and $CaOH^+$ were included in the analysis, and it was concluded that the TOF-SIMS data could be used to fully differentiate between calcium phosphate phases. Finally, Yan et al. compared PO_3^-/PO_2^- and also $CaOH^+/Ca^+$ TOF-SIMS secondary ion ratios from several CaP phases[54] of pure powders with findings consistent with the earlier work of Chuseui et al. and Lu et al. In addition, however, Yan et al. compared the spectra of the pure powder phases with those of a plasma sprayed calcium phosphate coating. Differences in the PO_3^-/PO_2^- and $CaOH^+/Ca^+$ ratios were observed from the surface and from within the bulk of the coating (recorded as a powdered sample) for an unannealed sample, indicating differences in the calcium phosphate phases present at the coating surface and in the bulk. However, identification of the specific phase(s) present by comparison of the PO_3^-/PO_2^- and $CaOH^+/Ca^+$ ion ratios obtained from the various pure powders was inconclusive.

Figure 4a and b presents positive and negative ion TOF-SIMS spectra, respectively, of the RF magnetron sputtered calcium phosphate films of the composite substrates. The dominant peak at 40 amu in the positive ion spectrum of Figure 4a reveals that Ca^+ secondary ions were ejected from the deposited layer following bombardment of the sample with primary ions (Ga^+). Importantly, no gold atoms (Au^+ $m/z = 197$) were detected in the secondary ion spectrum. This result implies that the deposited layer completely covers the gold substrate (over the sampling area of ∼100 μm^2) and, further, that no significant amount of gold has diffused to the coating surface (within the penetration depth of static TOF-SIMS analysis of approximately 1−2 nm[64]). The small peaks at 56 and 57 amu are tentatively attributable to CaO^+ and $CaOH^+$ secondary ions,[54,58] respectively, the significance of which will be discussed later. Spectral peaks arising from copper are observed at 63 and 65 amu (Cu isotopes in natural abundance). The presence of copper in the deposited film is most likely to have arisen during the deposition procedure and to originate from the copper sample clamping ring. Additional peaks in the spectrum of Figure 4a are assigned to hydrocarbon[58,65] and siloxane surface contaminants.[66]

The negative ion TOF-SIMS spectrum, Figure 4b, reveals characteristic calcium phosphate peaks from O^- (16 amu), OH^- (17 amu), O_2^- (32 amu), PO_2^- (63 amu), and PO_3^- (79 amu) secondary ions.[54,57,58] Additional peaks in the spectrum are assigned to hydrocarbon and chlorine air borne contaminants in accordance with the observations of Lu et al.[58] The remaining unassigned peaks are assumed to originate from any number of air borne contaminants such as other $C_xH_yO_z^-$ species or inorganic materials, as have been observed by other workers.[67] As discussed above, the ratio of the intensities of PO_3^-/PO_2^- secondary ions has been used previously to differentiate between calcium phosphate phases.[54,57,58,61] Hydroxyapatite itself has been found by three different groups to give very similar PO_3^-/PO_2^- ratios, for example, of 0.75(±0.06).[54] However, even without a quantitative evaluation of the area under the phosphate peaks in Figure 4b, it is clear that the PO_3^-/PO_2^- ratio is well above 1. This finding indicates that the deposited calcium phosphate films of the composite substrates are not comprised of stoichiometric hydroxyapatite. Consistent with this result is the fact that the $CaOH^+/Ca^+$ peak intensity ratio of Figure 4a is of the order of 0.2, well below the literature value for hydroxyapatite of 0.46, as measured by Yan et al.[49] In fact, the $CaOH^+/Ca^+$ peak intensity ratio of Figure 4a is comparable to

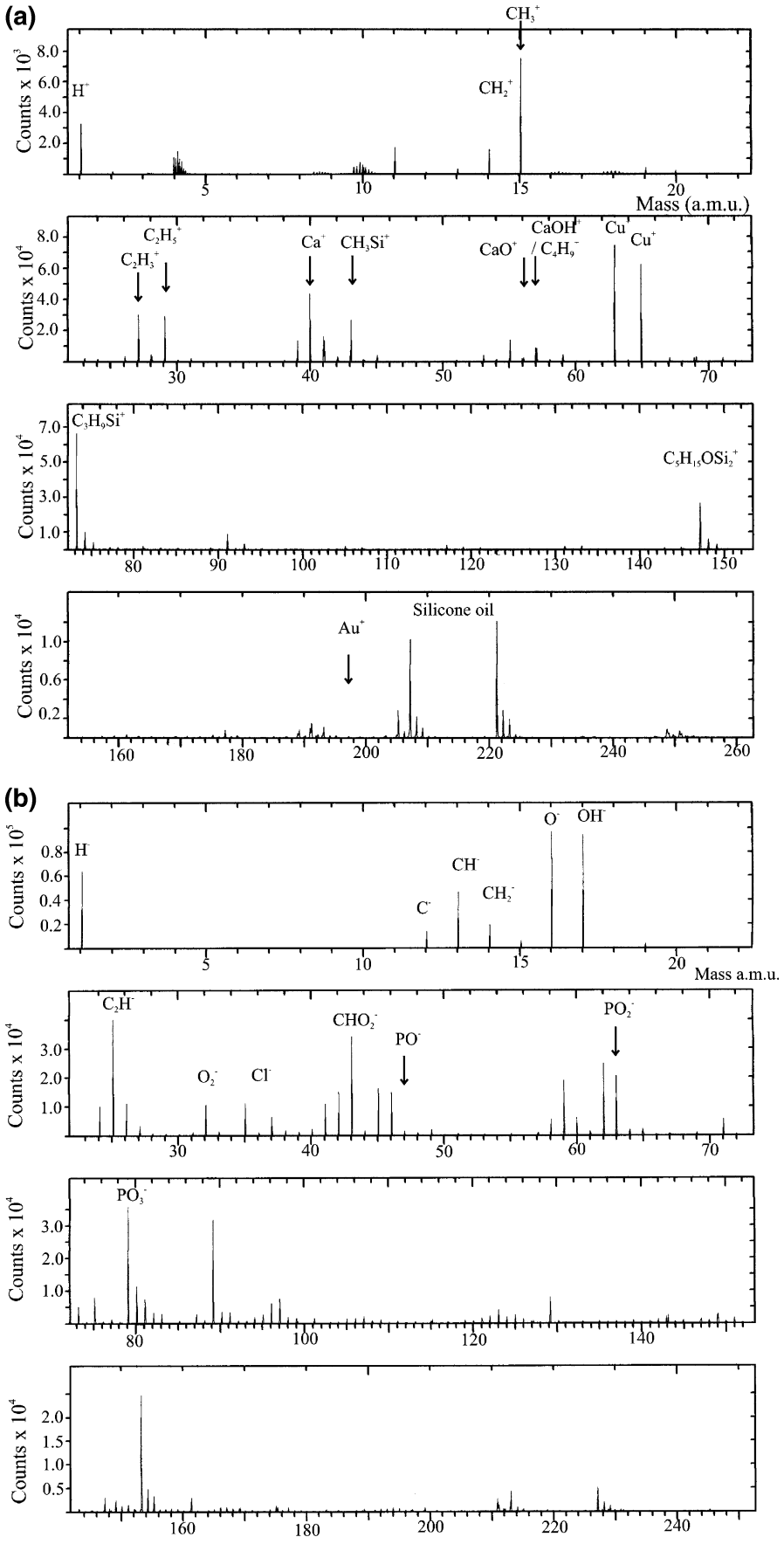

Figure 4. (a) Positive ion TOF-SIMS spectrum of the sputtered film recorded using Ga^+ primary ions incident over a surface area of 100 μm × 100 μm. The total primary ion count was 6.2×10^7, which is expected to be well within the static limit for TOF-SIMS analysis. (b) Negative ion TOF-SIMS spectrum recorded under conditions equivalent to that of (a).

that obtained for non-hydroxylated tricalcium phosphate powders of 0.22.[54]

Further interpretation of the TOF-SIMS spectra in terms of the calcium phosphate phases present in the sputtered layers is not feasible for several reasons. First, due to the presence of surface contaminants the intensity of several key peaks in the TOF-SIMS spectra may be influenced by additional counts and hence appear falsely high. For example, the $CaOH^+$ peak at 57 amu may be contaminated by $C_4H_9^+$ secondary ions, making the $CaOH^+/Ca^+$ ratio appear greater than it in fact is. Second, while the PO_3^-/PO_2^- ratio, for example, of the deposited films has been quantified, comparison with literature values is complicated by so-called "matrix effects", that is, the dependence of the proportion of secondary ions of a particular species detected upon its chemical environment.[64] Parameters contributing to matrix effects include the sample type (deposited film versus powder), the degree of crystallinity, the presence of more than one calcium phosphate phase, and the presence of surface contaminants. Third, in the current study, a different primary ion (Ga^+ rather than Cs^+), in addition to a different dosage, was employed relative to the literature studies, factors known to affect the ratios of detected species.[54]

Finally, a comment should be made with regard to the appearance of strong O^-, OH^-, and O_2^- peaks in the negative ion spectrum of Figure 4b. These peaks, and indeed the small $CaOH^+$ and CaO^+ peaks in the positive ion spectrum of Figure 4a, are not expected to arise in a non-hydroxylated calcium phosphate phase. Yan et al. attributed the appearance of $CaOH^+$ peaks in their non-hydroxylated calcium phosphate powder spectra to the presence of surface water.[54] An alternative explanation was proposed by Wen et al.,[62] who observed OH^- and O^- ions in TOF-SIMS spectra of the surfaces of HA layers while using dynamic TOF-SIMS employing more energetic primary ions and thereby probing deeper into the layers revealed that the amount of OH^- and O^- decreased. Wen et al. attributed these findings to a change in phase of the deposited material with depth from the surface; specifically, it was proposed that crystalline, hydroxylated hydroxyapatite was present at the surface of the coatings, while an amorphous phase existed within the film. This change in structure could conceivably occur due to different rates of cooling of the sputtered particles as they impacted either the metal substrate or the previously sputtered calcium phosphate material. To unambiguously determine the origin of the OH^- and O^- ions at the coating surfaces in the present work, a dynamic TOF-SIMS depth profile would have to be generated to investigate the changes in $CaOH^+/Ca^+$ and PO_3^-/PO_2^- ratios. Changes in these ratios would also indicate variations in calcium phosphate phases present as a function of depth probed. Such an experiment is, however, beyond the scope of the present study.

To summarize, the chemical composition of the sputtered films has been characterized via FTIR and TOF-SIMS. The dominance of phosphate bands in the infrared spectra and the detection of strong calcium peaks in the TOF-SIMS spectra indicate that the sputtered layer is predominantly calcium phosphate. It is likely that the CaP layer is present as a mixture of amorphous, non-hydroxylated phases rather than solely stoichiometric hydroxyapatite. However, it is not possible to comment on the exact CaP phases present due to the lack of a comprehensive study comparing powdered phases to RF magnetron sputtered layers by either FTIR or TOF-SIMS. In addition, surface contamination by hydrocarbon, siloxane, copper, and chlorine species was detected, a finding attributed to surface contamination during transport and the use of a copper clamping mechanism during deposition.

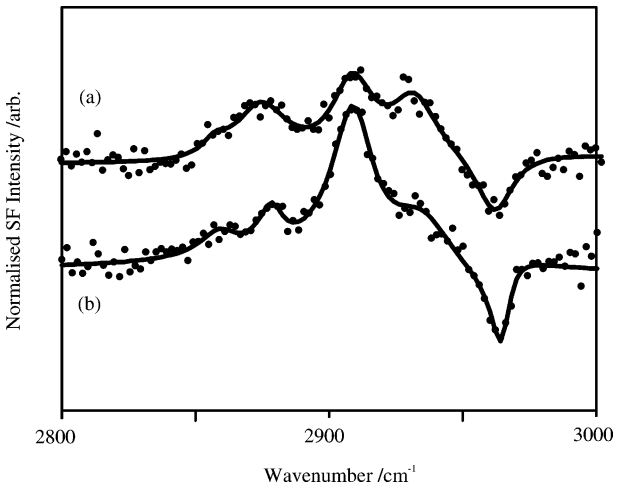

Figure 5. Sum frequency generation spectra of CDC. (a) Deposited by Langmuir Blodgett deposition onto the composite calcium phosphate/gold substrate. (b) Spin cast onto a gold-coated substrate to give a polymer layer thickness of 35 nm. Both spectra were recorded with p polarized sum frequency, visible and IR beams on a nanosecond spectrometer. The spectra have been displaced vertically for clarity. The sizes of the nonresonant backgrounds of the two spectra are different and depend on factors such as the Fresnel factors, which are difficult to quantify. Resonance assignments are given in ref 13.

Sum Frequency Generation Spectroscopy of CDC Films on the Composite Substrate. To demonstrate the suitability of the composite substrate for use in SFG spectroscopy, a spectrum of a monolayer of cetyl dimethicone copolyol (CDC) deposited via the Langmuir Blodgett technique on the CaP surface was recorded. The resulting SFG spectrum is presented in Figure 5a. Resonance assignments follow from earlier work on CDC SFG spectra[13] and only need summarizing here. The resonances at 2855 and 2877 cm^{-1} arise from the d^+ methylene symmetric stretching and the r^+ methyl symmetric stretching modes of the cetyl side chains of the polymer, respectively, while the resonance at 2933 cm^{-1} is assigned to a combination of Fermi resonance modes of the d^+ and r^+ modes of the alkyl chains. The 2968 cm^{-1} resonance is assigned to the r^- asymmetric stretching mode of the polydimethyl siloxane (PDMS) backbone and the cetyl side chains of the polymer. Finally, the resonance observed at 2908 cm^{-1} is assigned to the r^+ symmetric stretching mode of the PDMS backbone. The PEO side chains of CDC do not contribute to the SFG spectrum.

The appearance of the 2968 cm^{-1} resonance as a spectral dip in Figure 5a while the other resonances appear as spectral peaks is indicative of the presence of the interference effect described earlier arising from the spatial removal of the resonant CDC monolayer from the nonresonant gold surface via the incorporation of the intermediate CaP film. Indeed by application of the authors' previous theoretical and experimental analyses of thin film interference effects in related systems[13] (with modification of the refractive index of the substrate material to 1.64 for HA and use of the average CaP film thickness determined by ellipsometry of 44 nm), it is possible to predict that the observation of phases of $+90°$, that is, peaks for the r^+ modes, and $-90°$, that is, a dip, for the r^- resonance, corresponds to methyl groups oriented away from the surface at approximately 34.5° to the normal. Such a prediction is consistent with the alkyl side chains of CDC being oriented perpendicular to the interface (with their terminal methyl groups at 34.5° to the surface normal), and with the methyl groups of

the PDMS backbone oriented away from the substrate into air. Our previous work analyzing SFG spectra of varying thickness CDC films deposited directly onto gold substrates has indicated that this is in fact the preferred conformation of CDC in air. Further, comparison of a spectrum of a 35 nm thick CDC film deposited directly on gold, Figure 5b, with the spectrum of CDC deposited on a 45 nm thick CaP layer, Figure 5a, reveals that the two spectra are closely similar, as expected from the film thickness dependence of the interference effect. It should also be noted that the signal-to-noise ratio of the two spectra in Figure 5, recorded with a comparable number of scans, is similar. We have therefore demonstrated that SFG spectra of polymer films with good signal-to-noise ratios can be recorded using the composite substrate and can be interpreted using the existing interference model. Further analysis of molecular orientation and conformation of CDC films deposited on the composite substrate by the LB technique at different surface pressures will be presented in a later publication.

Conclusion

A novel substrate consisting of calcium phosphate sputter coated onto a gold film has been chemically and morphologically characterized. The coating is chemically different from the hydroxyapatite sputtering target and consists of amorphous, non-hydroxylated calcium phosphate. SFG spectra in air of cetyl dimethicone copolyol, a biocompatible polymer, adsorbed onto the calcium phosphate surface of the composite substrates have been measured and interpreted. The orientation of the polymer has been determined by comparison with SFG spectra of the polymer adsorbed directly on gold. Interference effects in the latter case have been analyzed previously, and hence the orientation of the polymer layers on gold/CaP substrates could be determined. The SFG spectra of CDC on the composite substrates were found to arise from hydrocarbon groups of the polymer backbone (CH_3) and from the cetyl side chains, both of which have a net orientation away from the substrate and toward air. The successful detection of SFG spectra of an adsorbed layer under air suggests that examining adsorption at the CaP substrate from aqueous solutions using SFG should be feasible and would represent a more appropriate system for biologically relevant applications.

Acknowledgment. S.J.M. gratefully acknowledges Procter & Gamble Technical Centers Limited, UK, and the EPSRC for the award of a CASE studentship. We also thank Dr. Mark Edwards and Dr. Chris White of Procter & Gamble Technical Centers Limited for useful discussions and for supplying the hydroxyapatite sputter target. Mr. Mark Bauer of Procter & Gamble Cincinnati, OH, and Mr. David Nichol of the Department of Material Sciences and Metallurgy, University of Cambridge, are thanked for their assistance with the TOF-SIMS and SEM measurements, respectively.

References and Notes

(1) Wang, J.; Buck, S. M.; Chen, Z. *J. Phys. Chem. B* **2002**, *106*, 11666−11672.
(2) Wang, J.; Buck, S. M.; Even, M. A.; Chen, Z. *J. Am. Chem. Soc.* **2002**, *124*, 13302−13305.
(3) Wang, J.; Buck, S. M.; Chen, Z. *Analyst* **2003**, *128*, 773−778.
(4) Wang, J.; Clarke, M. L.; Zhang, Y. B.; Chen, X. Y.; Chen, Z. *Langmuir* **2003**, *19*, 7862−7866.
(5) Kim, G.; Gurau, M.; Kim, J.; Cremer, P. S. *Langmuir* **2002**, *18*, 2807−2811.
(6) Chen, Z.; Ward, R.; Tian, Y.; Malizia, F.; Gracias, D. H.; Shen, Y. R.; Somorjai, G. A. *J. Biomed. Mater. Res.* **2002**, *62*, 254−264.
(7) Kim, J.; Somorjai, G. A. *J. Am. Chem. Soc.* **2003**, *125*, 3150−3158.
(8) Watry, M. R.; Richmond, G. L. *J. Phys. Chem. B* **2002**, *106*, 12517−12523.
(9) Lambert, A. G.; Neivandt, D. J.; Briggs, A. M.; Usadi, E. W.; Davies, P. B. *J. Phys. Chem. B* **2002**, *106*, 10693−10700.
(10) Lambert, A. G.; Neivandt, D. J.; Briggs, A. M.; Usadi, E. W.; Davies, P. B. *J. Phys. Chem. B* **2002**, *106*, 5461−5469.
(11) Holman, J.; Neivandt, D. J.; Davies, P. B. *Chem. Phys. Lett.* **2004**, *386*, 60−64.
(12) Holman, J.; Davies, P. B.; Neivandt, D. J. *J. Phys. Chem. B* **2004**, *108*, 1396−1404.
(13) McGall, S. J.; Davies, P. B.; Neivandt, D. J. *J. Phys. Chem. B* **2004**, *108*, 16030−16039.
(14) de Groot, K.; Wolke, J. G. C.; Jansen, J. A. *Proc.-Inst. Mech. Eng., Part H-J. Eng. Med.* **1998**, *212*, 137−147.
(15) van Dijk, K.; Schaeken, H. G.; Wolke, J. C. G.; Maree, C. H. M.; Habraken, F. H. P. M.; Verhoeven, J.; Jansen, J. A. *J. Biomed. Mater. Res.* **1995**, *29*, 269−276.
(16) Yamashita, K.; Yagi, T.; Umegaki, T. *J. Am. Ceram. Soc.* **1996**, *79*, 3313−3316.
(17) van Dijk, K.; Schaeken, H. G.; Wolke, J. G. C.; Jansen, J. A. *Biomaterials* **1996**, *17*, 405−410.
(18) van Dijk, K.; Maree, C. H. M.; Verhoeven, J.; Habraken, F. H. P. M.; Jansen, J. A. *J. Biomed. Mater. Res.* **1998**, *42*, 266−271.
(19) Wolke, J. G. C.; Vandijk, K.; Schaeken, H. G.; Degroot, K.; Jansen, J. A. *J. Biomed. Mater. Res.* **1994**, *28*, 1477−1484.
(20) van Dijk, K.; Schaeken, H. G.; Maree, C. H. M.; Verhoeven, J.; Wolke, J. C. G.; Habraken, F. H. P. M.; Jansen, J. A. *Surf. Coat. Technol.* **1995**, *76*, 206−210.
(21) van Dijk, K.; Verhoeven, J.; Maree, C. H. M.; Habraken, F. H. P. M.; Jansen, J. A. *Thin Solid Films* **1997**, *304*, 191−195.
(22) Hulshoff, J. E. G.; Hayakawa, T.; van Dijk, K.; Leijdekkersgovers, A. F. M.; van der Waerden, J. P. C. M.; Jansen, J. A. *J. Biomed. Mater. Res.* **1997**, *36*, 75−83.
(23) Hulshoff, J. E. G.; Jansen, J. A.; Kalk, W. *J. Dent. Res.* **1995**, *74*, 415−415.
(24) Hulshoff, J. E. G.; van Dijk, K.; de Ruijter, J. E.; Rietveld, F. J. R.; Ginsel, L. A.; Jansen, J. A. *J. Biomed. Mater. Res.* **1998**, *40*, 464−474.
(25) Hulshoff, J. E. G.; van Dijk, K.; van der Waerden, J. P. C. M.; Wolke, J. G. C.; Ginsel, L. A.; Jansen, J. A. *J. Biomed. Mater. Res.* **1995**, *29*, 967−975.
(26) Love, E. R.; Weimper, M.; Boyd, A.; Akay, M.; Meenan, B. J. *Key Eng. Mater.* **2000**, *192*−*195*, 255−258.
(27) Edwards, M. I.; Hughes, I. A. Method for treating dentures. *U.S. Patent Document*; The Procter & Gamble Co.: U.S., 2001.
(28) Hughes, I. A.; Edwards, M. I. Oral compositions. *U.S. Patent Document*; The Procter & Gamble Co.: U.S., 1999.
(29) Perloff, A.; Posner, A. S. *Science* **1956**, *124*, 583−584.
(30) Hind, A. R.; Bhargava, S. K.; McKinnon, A. *Adv. Colloid Interface Sci.* **2001**, *93*, 91−114.
(31) Bauer, M. 2003, personal communication.
(32) Lambert, A. G. Ph.D. Thesis, University of Cambridge, 2001.
(33) Bain, C. D.; Davies, P. B.; Ong, T. H.; Ward, R. N.; Brown, M. A. *Langmuir* **1991**, *7*, 1563−1566.
(34) Ong, T. H.; Davies, P. B.; Bain, C. D. *J. Phys. Chem.* **1993**, *97*, 12047−12050.
(35) Ward, R. N.; Davies, P. B.; Bain, C. D. *J. Phys. Chem.* **1993**, *97*, 7141−7143.
(36) Duffy, D. C.; Davies, P. B.; Creeth, A. M. *Langmuir* **1995**, *11*, 2931−2937.
(37) Johal, M. S.; Ward, R. N.; Davies, P. B. *J. Phys. Chem.* **1996**, *100*, 274−279.
(38) Windsor, R.; Neivandt, D. J.; Davies, P. B. *Langmuir* **2001**, *17*, 7306−7312.
(39) Casford, M. T. L.; Davies, P. B.; Neivandt, D. J. *Langmuir* **2003**, *19*, 7386−7391.
(40) McGall, S. J.; Davies, P. B.; Neivandt, D. J. *J. Phys. Chem. B* **2003**, *107*, 4718−4726.
(41) Hegner, M.; Wagner, P.; Semenza, G. *Surf. Sci.* **1993**, *291*, 39−46.
(42) Wagner, P.; Hegner, M.; Güntherodt, H.-J. *Langmuir* **1995**, *11*, 3867−3875.
(43) Stoch, A.; Brozek, A.; Blazewicz, S.; Jastrzebski, W.; Stoch, J.; Adamczyk, A.; Roj, E. *J. Mol. Struct.* **2003**, *651*, 389−396.
(44) Xie, J.; Riley, C.; Kumar, M.; Chittur, K. *Biomaterials* **2002**, *23*, 3609−3616.
(45) Zeng, H. T.; Lacefield, W. R. *Biomaterials* **2000**, *21*, 23−30.
(46) Park, E.; Condrate, R. A.; Lee, D. *Mater. Lett.* **1998**, *36*, 38−43.
(47) Meenan, B. J.; Boyd, A.; Love, E.; Akay, M. *Bioceramics*; Trans Tech Publications Ltd.: Zurich-Uetikon, 2000; pp 15−18.
(48) Lo, W. J.; Grant, D. M.; Ball, M. D.; Welsh, B. S.; Howdle, S. M.; Antonov, E. N.; Bagratashvili, V. N.; Popov, V. K. *J. Biomed. Mater. Res.* **2000**, *50*, 536−545.

(49) Wolke, J. G. C.; van der Waerden, J.; Schaeken, H. G.; Jansen, J. A. *Biomaterials* **2003**, *24*, 2623−2629.

(50) Chassot, E.; Oudadesse, H.; Irigaray, J.; Curis, E.; Benazeth, S.; Nicolis, I. *J. Appl. Phys.* **2001**, *90*, 6440−6446.

(51) Taddei, P.; Tinti, A.; Bottura, G.; Bertoluzza, A. *Biopolymers* **2000**, *57*, 140−148.

(52) Slosarczyk, A.; Paluszkiewicz, C.; Gawlicki, M.; Paszkiewicz, Z. *Ceram. Int.* **1997**, *23*, 297−304.

(53) Wolke, J. G. C.; vanderWaerden, J.; deGroot, K.; Jansen, J. A. *Biomaterials* **1997**, *18*, 483−488.

(54) Yan, L. L.; Leng, Y.; Weng, L. T. *Biomaterials* **2003**, *24*, 2585−2592.

(55) Carayon, M. T.; Lacout, J. L. *J. Solid State Chem.* **2003**, *172*, 339−350.

(56) Leadley, S. R.; Davies, M. C.; Ribeiro, C. C.; Barbosa, M. A.; Paul, A. J.; Watts, J. F. *Biomaterials* **1997**, *18*, 311−316.

(57) Chusuei, C. C.; Goodman, D. W.; Van Stipdonk, M. J.; Justes, D. R.; Schweikert, E. A. *Anal. Chem.* **1999**, *71*, 149−153.

(58) Lu, H. B.; Campbell, C. T.; Graham, D. J.; Ratner, B. D. *Anal. Chem.* **2000**, *72*, 2886−2894.

(59) Haddow, D. B.; James, P. F.; VanNoort, R. *J. Mater. Sci.: Mater. Med.* **1996**, *7*, 255−260.

(60) Allen, G. C.; Ciliberto, E.; Fragala, I.; Spoto, G. *Nucl. Instrum. Methods Phys. Res., Sect. B* **1996**, *116*, 457−460.

(61) Chusuei, C. C.; Goodman, D. W.; Van Stipdonk, M. J.; Justes, D. R.; Loh, K. H.; Schweikert, E. A. *Langmuir* **1999**, *15*, 7355−7360.

(62) Wen, J.; Leng, Y.; Chen, J. Y.; Zhang, C. *Biomaterials* **2000**, *21*, 1339−1343.

(63) Ni, M.; Ratner, B. D. *Biomaterials* **2003**, *24*, 4323−4331.

(64) Belu, A. M.; Graham, D. J.; Castner, D. G. *Biomaterials* **2003**, *24*, 3635−3653.

(65) Viornery, C.; Chevolot, Y.; Leonard, D.; Aronsson, B. O.; Pechy, P.; Mathieu, H. J.; Descouts, P.; Gratzel, M. *Langmuir* **2002**, *18*, 2582−2589.

(66) Clarson, S. J.; Stuart, J. O.; Selby, C. E.; Sabata, A.; Smith, S. D.; Ashraf, A. *Macromolecules* **1995**, *28*, 674−677.

(67) Schnabel, P. H.; Lindley, P. M.; Nehrkorn, D.; Kendall, M. *Semicond. Fabr.: Technol. Metrol.* **2000**, *11*, 123−129.